Received: 2 May 2020 | Revised: 12 July 2020 | Accepted: 29 July 2020

DOI: 10.1096/fj.202001046R

RESEARCH ARTICLE

THE FASEB JOURNAL

Protein synthesis is suppressed in sporadic and familial Parkinson's disease by LRRK2

Prasannakumar Deshpande[1] | Dani Flinkman[1,2] | Ye Hong[1] | Elena Goltseva[2] | Valentina Siino[2] | Lihua Sun[1] | Sirkku Peltonen[3] | Laura L. Elo[1] | Valtteri Kaasinen[4] | Peter James[1,2] | Eleanor T. Coffey[1]

[1]Turku Bioscience, University of Turku and Åbo Akademi University, Turku, Finland

[2]Department of Immunotechnology, Lund University, Lund, Sweden

[3]Department of Dermatology, University of Turku and Turku University Hospital, Turku, Finland

[4]Division of Clinical Neurosciences, Turku University Hospital and University of Turku, Turku, Finland

Correspondence
Eleanor T. Coffey, Turku Bioscience, University of Turku and Åbo Akademi University, Turku, Finland.
Email: eleanor.coffey@bioscience.fi

Funding information
Business Finland; Michael J. Fox Foundation for Parkinson's Research (MJFF); Åbo Akademi University; Turku Graduate School of Biomedical Sciences; MATTI Graduate School; University of Lund

Abstract

Gain of function LRRK2-G2019S is the most frequent mutation found in familial and sporadic Parkinson's disease. It is expected therefore that understanding the cellular function of LRRK2 will provide insight on the pathological mechanism not only of inherited Parkinson's, but also of sporadic Parkinson's, the more common form. Here, we show that constitutive LRRK2 activity controls nascent protein synthesis in rodent neurons. Specifically, pharmacological inhibition of LRRK2, *Lrrk2* knockdown or *Lrrk2* knockout, all lead to increased translation. In the rotenone model for sporadic Parkinson's, LRRK2 activity increases, dopaminergic neuron translation decreases, and the neurites atrophy. All are prevented by LRRK2 inhibitors. Moreover, in striatum and substantia nigra of rotenone treated rats, phosphorylation changes are observed on eIF2α-S52(↑), eIF2s2-S2(↓), and eEF2-T57(↑) in directions that signify protein synthesis arrest. Significantly, translation is reduced by 40% in fibroblasts from Parkinson's patients (G2019S and sporadic cases alike) and this is reversed upon LRRK2 inhibitor treatment. In cells from multiple system atrophy patients, translation is unchanged suggesting that repression of translation is specific to Parkinson's disease. These findings indicate that repression of translation is a proximal function of LRRK2 in Parkinson's pathology.

KEYWORDS

biomarker, cellular mechanism, eEF2, LRRK2, neurodegeneration, Parkinson's disease

Abbreviations: [35]S-met, [35]S-methionine; ACN, acetonitrile; AHA, L-azidohomoalanine; DIV, days in vitro; DMSO, dimethyl sulfoxide; EDTA, ethylenediaminetetraacetic acid; eEF, Eukaryotic elongation factor; EGTA, ethylene glycol-bis(β-aminoethyl ether)-N,N,N′,N′-tetraacetic acid; eIF, Eukaryotic initiation factor; FC, fold change; FDR, false discovery rate; Gln, L-glutamine; HPLC, high-performance liquid chromatography; HRP, horseradish peroxidase; IRES, Internal Ribosome Entry Site; KO, knockout; LC, liquid chromatography; LRRK2, leucine rich-repeat kinase 2; MEM, minimal essential medium; Met, methionine; MS, mass spectrometry; MSA, multiple system atrophy; NINDS, National Institute of Neurological Disorders; NTG, non-targeting; PFA, paraformaldehyde; PMSF, phenylmethylsulfonyl fluoride; PD, Parkinson's disease; ROC, receiver operating characteristic; r.o.i., regions of interests; RT, room temperature; SEM, standard error of the mean; SNpc, substantia nigra pars compacta; TBST, tris-buffered saline with 0.01% tween; TFA, trifluoroacetic acid; TH, tyrosine hydroxylase; TNGB, Telethon Network of Genetics Biobanks; TUH, Turku University Hospital; WT, wild type; 4E-BP1, eukaryotic translation initiation factor 4E-binding protein 1; 6-OHDA, 6-hydroxydopamine.

1 | INTRODUCTION

Parkinson's disease is the second most common neurodegenerative disorder after Alzheimer's disease with the highest prevalence in Europe and North and South America.[1,2] No cure exists and long term symptomatic treatment is associated with complications. Although its neuropathological basis is not fully understood, degeneration of dopaminergic neurons in the substantia nigra pars compacta (SNpc) is repeatedly shown, and subsequent reduction of dopamine release in the basal ganglia leads to Parkinsonian motor symptoms.[2] Meta-analysis of genes associated with Parkinson's disease has revealed over 40 risk loci.[3] Among these, leucine rich-repeat kinase 2 (*LRRK2*)-*G2019S* is the most common mutation and is associated with late onset Parkinson's disease. *LRRK2*-G2019S confers a gain of function in kinase activity,[4] as do disease-associated mutations in the GTPase domain.[5-7] In addition to its association with familial Parkinson's, genome-wide association studies have highlighted *LRRK2* as a risk factor for sporadic Parkinson's.[8] Because of this and the finding that *LRRK2-G2019S* cases are symptomatically indistinguishable from sporadic ones,[9-11] it has been proposed that LRRK2 may contribute to the pathology of sporadic Parkinson's disease.[12] Therefore, identifying the cellular function of LRRK2 is expected to help elucidate the pathological mechanism of sporadic Parkinson's disease, which accounts for around 90% of all cases.

With regards to what is already known about LRRK2 function, a large body of evidence suggests that LRRK2 regulates endolysosomal trafficking and that this may contribute to the pathology of Parkinson's disease.[13-16] In addition to this, LRRK2-G2019S has been implicated in the dysregulation of protein synthesis through the phosphorylation of ribosomal proteins and regulators of ribosomal function, suggesting that LRRK2 augments RNA translation.[17-20] However, this is in conflict with postmortem data from Parkinson's patients where eIF2α and eEF2 phosphorylation changes indicate that protein synthesis is repressed.[21,22] Also, expression levels of regulators of endolysosomal trafficking (VPS35, Gcase1, LAMP2A, and ATP13A2) are decreased in postmortem brains from Parkinson's patients carrying LRRK2 mutations.[13,15] Despite the supporting clinical data, the possibility that LRRK2 could suppress translation has not received much attention.

Here we took a basic discovery approach to identify what type of brain organelle was most highly phosphorylated by the disease-associated LRRK2-G2019S. This highlighted that ribosomal fractions were preferentially phosphorylated and prompted us to examine whether endogenous LRRK2 regulated RNA translation. We found that translation was decreased in both the rotenone and 6-hydroxy dopamine models of Parkinson's disease. Moreover, when we examined fibroblast cells isolated from sporadic and G2019S patients, we found that translation was decreased compared to healthy individuals, but increased following treatment with LRRK2 inhibitors. A shot-gun phospho-proteomic analysis combined with antibody validation revealed that checkpoint regulators of protein synthesis arrest were switched on in substantia nigra and striatum of the rotenone rat model of Parkinson's and in cells from sporadic patients. These data imply that protein synthesis is repressed in sporadic Parkinson's disease by a LRRK2-dependent mechanism.

2 | MATERIALS AND METHODS

2.1 | Antibodies, tools

Antibodies for LRRK2 [MJFF2 (C41-2)] (# ab133474), phospho-S935-LRRK2 [UDD2 10 (12)] (#ab133450), phospho-T73-Rab10 [MJF-R21] (# ab230261), Rab10 [MJF-R23] (# ab237703), and RPL10a (# ab55544) were from Abcam. Anti-tyrosine hydroxylase was from Millipore (#AB1542). Antibodies for eIF2B5(sc-28854), eIF2α (sc-11386), phospho-eIF2α–S52 (sc-101670), eIF4G3 (sc-100732), and Ndufs3 (sc-292169) were from Santa Cruz Biotechnology. Anti-Rab8 (#R66320) and Rab4 (#R68520) were from BD Transduction Laboratories. Anti-4E-BP1 (#9452), eEF2 (#2332) and phospho-eEF2(T57) (#2331) were from Cell Signaling Technology and anti-actin (# A3853) was from Sigma-Aldrich. LRRK2-IN1 was from Merck Millipore (# 438193), GSK-2578215A (#4629) and MLi-2 (# 5756) were from Tocris Bioscience. Miglyol 812N was from Cemer Oleo, GmbH, and Co, KG (Germany). Patient cells were from the National Institute of Neurological Disorders and Stroke (NINDS) repository at the Coriell Institute for Medical Research and the Cell Line and DNA Biobank from Patients Affected by Genetic Diseases, Telethon Network of Genetic Biobanks (TNGB) (project no. GTB12001).[23] C57BL/6-*Lrrk2*$^{tm1.1Mjff}$/J mice developed by Michael J. Fox Foundation[24] were obtained from The Jackson Laboratory (Stock no. 016121).

2.2 | Plasmid

The bicistronic CAP/IRES reporter(pYIC) was a gift from Han Htun.[25]

2.3 | Separation of mitochondrial and ribosomal fractions

Mitochondrial and ribosomal fractions were isolated from rat brain as previously.[26] Briefly, rat brains were

homogenized in 12 mL homogenization buffer (300 mM sucrose, 10 mM HEPES, pH 7.4, 0.1 mM EGTA, and 2 mM EDTA) with protease inhibitors (1 μg/ml leupeptin, pepstatin, and aprotinin and 100 μg/mL PMSF). Lysate was kept on ice for 20 minutes and unbroken cells (P1) were removed by centrifugation at 2800*g*avg for 10 minutes at 4°C. Supernatant 1 (S1) was centrifuged at 22 000*g*avg at 4°C for 10 minutes using a SW41Ti rotor and Beckman L90K ultracentrifuge. The subsequent pellet (P2) contained mitochondria. The remaining supernatant 2 (S2) was centrifuged at 100 000*g*avg at 4°C for 8 hours to give pellet 3 (P3), which contained ribosomes.

2.4 | Sucrose gradient fractionation of ribosomal subunits

P14 rat brain was homogenized with a Potter-Elvehjem homogenizer (20 strokes) in 5 mL of ice-cold homogenization buffer (5% sucrose, 10 mM HEPES, pH7.4, 0.1 mM EGTA, and 2 mM EDTA) with protease inhibitors (as above) and the second supernatant (S2) fraction was prepared as before. S2 was loaded on a linear sucrose gradient (5%-50% in 8 mL). The gradient was centrifuged at 150 000*g* at 4°C in a SW41Ti rotor for 2 hours and 40 minutes. Fractions of 0.5 mL were collected from the bottom of the tube using a peristaltic pump and RNA amount was determined by measuring absorbance at 260 nm.

2.5 | In vitro phosphorylation of brain fractions using LRRK2-G2019S

The assay was carried out as previously with modifications.[27] Briefly, the P3 ribosomal pellet or the P2 mitochondrial pellet from P7 rat brain were resuspended in equal volume of buffer (20 mM MOPS, pH 7.2, 2 mM EGTA, 2 mM EDTA, 10% glycerol, and 1 mM benzamidine) with protease inhibitors (1 μg/mL leupeptin, pepstatin, and aprotinin and 100 μg/mL PMSF) and 1% IGEPAL. After 5 minutes on ice, the lysate was homogenized with 8 strokes using a 27G syringe, and then, centrifuged at 16 000*g* at 4°C. About 0.1 mM ZnCl2 and 2.5 U Antarctic phosphatase (New England Biolabs) were added to the supernatant and incubated at 37°C for 2 hours followed by heat inactivation of phosphatase at 65°C, 10 minutes. Lysates were desalted using Micro Biospin columns from Biorad (catalogue # 732-6223). To start the kinase reaction, 5 μCi of γ-[32P] ATP, MgCl2 (10 mM) and 44.12 nM LRRK2-G2019S (Invitrogen, cat# PV4881) was added. Reactions were carried out at 30°C for 1 hour and ended by adding *Laemmli* buffer. Radioactive samples were separated by SDS-PAGE and visualized by autoradiography.

2.6 | Hippocampal and midbrain cultures

Hippocampal neurons were isolated from new born Sprague-Dawley rats as previously described[28] and used at 12 days post plating. *Lrrk2* knockout and wild-type neurons were litter matched from *Lrrk2* ± breeding pairs. Genotyping was done on cell lysates following Jackson Laboratory recommendations. Midbrain cultures were isolated from newborn Sprague Dawley rats or C57BL6 mice as indicated. Midbrains in dissection medium (30 mM K_2SO_4, 81.8 mM Na_2SO_4, 5.8 mM $MgCl_2$, 1 mM D-glucose, 0.25 mM Hepes pH 7.4, 0.001% Phenol red, and supplemented with 1 μM kynurenic acid) were digested with Papain (10 U/mL Worthington, 3119) as previously described.[29] Plating density is indicated in subsequent paragraphs. Cells were maintained in Neurobasal A (Gibco, Life Technologies) supplemented with B27, 2 mM Gln and penicillin 50 U/mL and streptomycin 50 μg/mL and used at 3 and 12 days post plating for IN1 and MLi inhibitor analyses.

2.7 | Patient skin cell isolation and maintenance

Skin punches were taken from the upper arm of donors and patients by a licensed dermatologist at Turku University Hospital (TUH). Punches were placed immediately in *Minimal essential medium* (MEM, Sigma Aldrich). Tissue was chopped into several small pieces using a sterile blade and incubated in MEM supplemented with Gln (2 mM), penicillin (50 U/mL), and streptomycin (50 μg/mL) at 37°C, 5% CO2. Fibroblasts were passaged when 95% confluent. Experiments were done at passage 7 to 9.

2.8 | Neurite atrophy measurement

Midbrain cultures (200 000 cells/well in 96 well plate) were treated at 3 days post-plating with rotenone in DMSO ± LRRK2 inhibitors (IN1, GSK2578215A or MLi-2) as indicated in the figures. After 24 hours, cells were fixed with 4% PFA in PBS. To identify dopaminergic neurons, tyrosine hydroxylase (TH) was detected by immunostaining as previously described.[30] Cells were imaged with a Zeiss TIRF-3 microscope equipped with CMOS Orca Flash 4 (Hamamatsu). All TH-positive cells were counted from tiled images of wells. The number of TH-positive cells that had intact neurites (>2× soma diameter) were counted and expressed as a percentage of all TH-positive cells. To avoid false positive scoring of neurite atrophy, the intensity of TH images was saturated during scoring, so that if neurites were visible if present, even in cells with lower TH expression, as shown in S4D.

2.9 | Cell death measurement

Neuronal pyknosis was evaluated from TH-positive cells using 4 μg/mL Hoechst-33342. Tile images of nuclei and TH fluorescence were acquired using a Zeiss AxioVert 200M microscope and 10× objective. All TH-positive cells were scored by a blinded experimenter. Cells with shrunken, bright nuclei were considered pyknotic.

2.10 | 6-OHDA treatment

Freshly prepared 6-OHDA (40 mM) in DMSO was added to 3 days in vitro midbrain cells plated at 150 000 cells/well in a 96 well plate. First, 180 μL of fresh medium was added. Then 6-OHDA was added to a final concentration of 40 μM with 0.2% ascorbic acid in 20 μL medium. After 15 minutes, cells were washed 1× with medium and 50 nM MLi-2 or 0.1% DMSO was added. After 24 hours, AHA labeling was performed and cells were stained for TH to enable analysis of protein synthesis in dopaminergic neurons.

2.11 | Measurement of translation using AHA labelling

AHA labelling was carried out as previously, with modifications.[31] Briefly, hippocampal, midbrain or skin cells were plated at densities of 100 000, 500 000 or 50 000 cells per well on round coverslips (1.3 cm diameter). At 20 days in vitro (hippocampal), 12 days (dopaminergic) or 48 hours post-plating (skin), cells were washed 1× and incubated with Met-free DMEM (Gibco, Thermo Fisher Scientific) supplemented with 2 mM Gln for 30 minutes including LRRK2 inhibitors or 0.1% DMSO, followed by Met-free media containing 1 mM L-azidohomoalanine (AHA) + LRRK2 inhibitors/DMSO. Labeling was stopped by washing with 1 mL PBS followed by fixation in 4% paraformaldehyde. Cells were permeablized overnight in *block* (0.25% Triton X100, 0.2% BSA, 5% sucrose, and 10% horse serum in PBS), and washed 5× with 1 mL of 3% BSA in PBS. Cycloaddition of Alexa-488 was carried out using the Thermo Fisher Scientific kit (catalogue # A10267) according to the manufacturer's instructions. Nuclei were stained with 1:2000 Hoechst-33342 in PBS. Coverslips were divided into four quadrants and three to five fluorescent images were acquired per quadrant using a 40× objective and a Leica DMRE microscope with an ORCA C4742-95 CCD camera (Hamamatsu). Mean fluorescence intensity r.o.i.s in the soma were measured from all cells using ImageJ. Background was determined from identical r.o.i. from cells that did not receive AHA, as previously.[32] For dendrites, line intensity measurements were taken from 10 μm lines positioned at the soma and extending into a primary dendrite. Image acquisition settings were identical for all samples and analysis was performed by an experimenter that was blinded to the treatment. Specifically, slide labels were masked by an uninvolved researcher and assigned code numbers, which were only revealed upon completion of analysis.

2.12 | Measurement of translation using $^{[35]}$S-Met labelling

Hippocampal neurons (50 000 cells/well on 48 well plates) were depleted of Met in Met-free DMEM supplemented with 2 mM L-Gln at 20 days post plating for 30 minutes ± anisomycin or MLi-2 as indicated. $^{[35]}$S-Met was added to a final concentration of 200 μCi/mL, for 60 minutes. After labeling, cells were lysed in *Laemmli* buffer and proteins separated by SDS-PAGE. $^{[35]}$S-Met incorporation was detected using a Fuji phosphorimager and intensities quantified using ImageJ for the entire gel lane of proteins and normalized to coomassie blue.

2.13 | Measurement of translation in a reconstituted assay

A human, cell-free protein expression system from Takara Bio Inc (Japan) was used according to the manufacturer's instructions. Briefly, a β-galactosidase reporter (150 ng) was incubated with 60 nM GST-G2019S-LRRK2 or GST alone for 1.5 hours at 32°C. β-galactosidase expression was measured using colorimetric detection ($Abs_{420\,nm}$, using a Synergy H1 plate reader (Biotek) from samples in a 96-well plate. Absorbance at 420 nm was measured using the Synergy H1 Hybrid Reader (Biotek).

2.14 | Gene knockdown

Gene silencing was carried out as previously.[32] Specifically, 6 days in vitro hippocampal neurons on coverslips were transfected with 200 nM non-targeting (5′-GCUAAUACCUAUCAAUUGUU-3′) or *Lrrk2* siRNA (5′-AAGUUGAUAGUCAGGCUGAAU-3′)[33] and protein synthesis was measured using AHA labeling at 20 days in vitro. The efficiency of knockdown was assessed by immunostaining using the LRRK2 antibody [MJFF2 (C41-2)] (# ab133474, Abcam) at1:200 dilution, and secondary detection was with goat anti-Rabbit IgG (H + L)-Alexa Fluor 568 (#A11011, ThermoFisher Scientific) at 1:500 dilution. Fluorescence intensity of regions of interest in soma and dendrites was measured as described above by a blinded experimenter.

2.15 | ATP measurements

Neurons from P0 rat cortex were plated at 150 000 cells per well in glass bottomed 96-well plates (Greiner) in

200 μL of medium. At DIV7, ATP was measured using the CellTiterGlo reagent (Promega) in an Envision Multilabel reader (PerkinElmer).

2.16 | Rotenone treatment of rats and behavioral testing

Group housed female, 12 weeks old Sprague-Dawley rats were injected intraperitoneally with rotenone (n = 6) (1 mg/kg) diluted in carrier (98% Miglyol 812N, 2% DMSO), or with carrier alone (n = 6). Postural instability was tested at 6 and 11 days according to a previous report.[34] Briefly, while holding the animal vertically, one forelimb was immobilized to the chest while the other forelimb touched the surface of scored sandpaper. The center of gravity of the animal was advanced until a step was triggered. The average distance taken to trigger a step was measured from both forelimbs. The test was performed between 9 and 11 AM before the start of injections (0 day), mid-way (6 days) and one day before termination (11 days) by a blinded experimenter. On 12 days, animals underwent terminal anesthesia (150 mg/kg of Mebunat intraperitoneal; Orion Corporation). Brains were rapidly isolated and cut into 1 mm thick coronal sections starting rostral to the optic chiasm and continuing until midway through the pons, using a pre-chilled rat brain matrix (Zivic Instruments) as described previously.[35] Sections were frozen on dry ice and striatum and substantia nigra were manually dissected using a scalpel.[36] Tissues were denatured using Denator (Denator, Uppsala, Sweden) before storage at −80°C.

2.17 | Phosphopeptide enrichment and mass spectrometry sample analysis

For analysis of phosphoprotein changes in substantia nigra and striatum of rotenone-treated rats, animals were treated exactly as described above. Chemicals for digestion and mass spectrometry analysis were from Sigma-Aldrich (St. Louis, USA) unless otherwise stated. Substantia nigra or striatum from rotenone injected (n = 14) or control (n = 12) rats were run 1 cm into a SDS-PAGE, and stained using GelCode blue (Thermo Fisher Scientific). Concentrated samples were excised from the gel, cut in 1 mm^3 pieces, and destained with 40 mM Ambic/50% for 3 × 15 minutes. Samples were reduced with 20 mM DTT for 30 minutes at 56°C, and alkylated with 55 mM Iodoacetoamide for 20 minutes at RT in the dark. Trypsin digestion was performed overnight with sequencing grade modified Trypsin (Promega, Madison, Wisconsin, USA). Peptides were extracted with 100% ACN and 50% ACN/5% HCOOH, and dried using a SpeedVac for ~2 hours. Dried peptides were resuspended in 10 μL 0.1% TFA, followed by addition of 40 μL of 6% TFA 80% ACN and loaded on a column consisting of 1 mg of 20 μM, 300Å TiO2 particles (ZirChrom, Anoka, MN, USA) by centrifugation at 3000 rpm for 45 seconds. Columns were washed twice with 50 μL of 6% TFA/80% ACN, and twice with 50 μL of 0.1% TFA. Centrifugation was at 3000 rpm for 30 seconds between washes. Peptides were eluted with 50 μL of 5% NH_4OH, and acidified with 100 μL of 10% HCOOH and cleaned using in-house prepared C18 spin columns, and dried with a SpeedVac at RT for ~30 minutes. Enriched phosphopeptides were resuspended in 15 μL of 0.1% HCOOH, and analysis was carried out using an LC-ESI-MS/MS with an Easy-nLC1200 coupled to an Orbitrap Fusion Lumos (Thermo Fisher Scientific) operated in Data-Dependent Acquisition mode with 3 seconds cycle time and EThcD collision. Survey scans were acquired at 120 K resolution at 200 *m/z* with 375-1500 *m/z* scan range, and MS/MS at 30 K resolution at 200 *m/z*. Peptides were first loaded on a 100 μM × 2 cm trapping column, and separated on 75 μM ID × 15 cm analytical column, which were packed with ReproSil-Pur 5 μm 200 Å C18-AQ (Dr Maisch HPLC GmbH, Ammerbuch-Entringen, Germany). Mobile phase A consisted of 0.1% FA, and B 80/20 (v/v) ACN/water, and peptides were eluted over a 60 minutes gradient at 300 nL/min.

2.18 | Data analysis from mass spectrometry output

MS/MS data analysis was carried out using MaxQuant v1.6.3.4[37] with *match between runs* and *known contaminants* selected. Data were searched against *Rattus norvegicus* UniprotKB database. Trypsin/P with two allowed miss-cleavages was used and FDR was set at 1% for proteins and peptides. Decoy-target FDR estimation in MaxQuant was used to determine false positives. Allowed modifications were fixed carbamidomethylation at C, variable M oxidation, STY phosphorylation and protein N-terminal acetylation. Data was log2 transformed and the resulting data was analyzed using Perseus v1.6.2.3.[38] Perseus-marked potential contaminants and phosphosites with more than 50% missing values in both rotenone and control conditions were removed. Samples were normalized by subtracting the sample median intensity from individual phosphosite intensities as previously described,[38,39] and the global median of all samples was added to each phosphosite intensity to bring phosphosite intensities back to their original scale. The Perseus *replace missing values from normal distribution* function was used. MS/MS statistical analysis used Student's *t* test ($P < .05$) with the Perseus *permutation based FDR for multiple hypothesis testing correction* set at FDR < 0.05. A threshold for significantly changing phosphosites of Log2 fold change of 1 was also imposed.

2.19 | Western blotting

After treatment, mouse hippocampal (DIV20) or midbrain (DIV8) neurons were lysed in 1× Laemmli (Biorad #1610747) supplemented with 1× protease inhibitor cocktail (#005892791001, Roche) and 2× phosphatase inhibitor cocktail (# P2850, Sigma), 2 mM $MgCl_2$ and 25 U/mL Benzonase (# 70746, Merck Millipore). Lysates were resolved on 4%-20% Mini-PROTEAN TGX Precast Protein Gels (#4561096, Biorad) Membranes or gels were cut in horizontal strips according to defined molecular weight and blocked with 5% milk in Tris-buffered saline with 0.01% tween (TBST) for 1 hour and probed with primary antibodies overnight at 4°C. Antibodies were used at the following dilutions, phospho-S935 LRRK2 (1:1000), LRRK2 (1:1000), RPL10a (1:10 000), 4E-BP1 (1:1000), phospho-4EBP (1:1000), eIF2B5 (1:500), NDUFS3 (1:500), Rab10 (1:3000), phospho-T73-Rab10 (1:1000), eIF2α (1:500), phospho-S52-eIF2α (1:500), phospho-T57-eEF2 (1:1000), eEF2 (1:1000), and actin (1:5000). Secondary antibodies, anti-rabbit IgG-HRP (1:5000, #7074, CST), or anti-mouse-HRP (1:10 000, #12-349, Merck Millipore) in TBST containing 5% milk for 1 hour at RT. Bands were detected with SuperSignal West Femto Maximum Sensitivity Substrate (#34095, ThermoFisher Scientific) and analyzed using the ChemiDoc MP (BIO-RAD). Densitometry was performed using Image Lab v6.0.1 (BIO-RAD).

For immunoblotting, patient and donor fibroblasts were grown on 10 cm dishes and lysed in 70 µL Laemmli (BIO_RAD) as described above. Protein concentration was determined using Pierce 660 nm Protein Assay Reagent (#22660, ThermoFisher Scientific) mixed with ionic detergent compatibility reagent (#22663, ThermoFisher Scientific). About 15 µg of protein was loaded onto 4%-20% gradient gels and samples were immunoblotted with antibodies against phospho-S395-LRRK2 and phospho-T57-eEF2 as above.

2.20 | Statistical analysis

Student's two-tailed *t* test or One-way ANOVA followed by post hoc Bonferroni corrections were used as indicated. For patient data, Student's *t* test was used followed by multiple comparison correction with the Benjamini and Hochberg method. Adjusted *P* values are shown. The receiver operating characteristic (ROC) curve and Pearson's correlation analysis were carried out using GraphPad Prism, and *P* values calculated by Student's *t* test. For the ROC curve, % sensitivity was calculated from: True positive * 100/number of PD individuals and % specificity was calculated from True negatives * 100/number of healthy individuals.

2.21 | Repository information and ethical permission for human samples

For patient biopsy donors in the Turku University Hospital (TUH) cohort, patient consent was obtained according to the Declaration of Helsinki and approved by an ethical committee at TUH. Patient and control skin fibroblasts from the NINDS cohort were from the NINDS Cell Line Repository (http://ccr.coriell.org/ninds). Patient and control skin fibroblasts from the TNGB cohort were from the "Cell Line and DNA Biobank from Patients Affected by Genetic Diseases," member of the Telethon Network of Genetic Biobanks (project no. GTB12001), funded by Telethon Italy.

2.22 | Data availability statement

Raw data will be made available upon request.

2.23 | Ethical approval

Animal procedures were approved by the Animal Experiment Board in Finland. Patient samples were taken with informed consent and the work was approved by Turku University Hospital (Permission # T175/2014).

3 | RESULTS

3.1 | Rat LRRK2 localizes to and phosphorylates ribosomal fractions

To determine which organelles pathologically active LRRK2-G2019S phosphorylated in brain, we did centrifugal separation of rat brain into fractions and phosphorylated them in vitro using purified LRRK2-G2019S. LRRK2-G2019S showed preferential phosphorylation of ribosome-enriched fractions (P3) (Figure 1A). Moreover, we found that 60% of endogenous brain LRRK2 co-purified with ribosomes and 20% with the mitochondrial fraction (P2) (Figures 1B,C and S1). We further resolved the ribosomal fraction using sucrose gradient centrifugation and used 40S (eIF2α, eIF2B5, and eIF4G3) and 60S (RPL10a) ribosomal subunit markers to validate the fractionation, as previously[40] (Figure 1D,E). This established that the bulk of endogenous LRRK2 localizes to the small 40S ribosomal subunits in brain (Figure 1D).

3.2 | LRRK2 suppresses RNA translation in dopaminergic and hippocampal neurons

As LRRK2 was enriched at small ribosomal subunits in brain, we tested whether LRRK2 regulated ribosomal

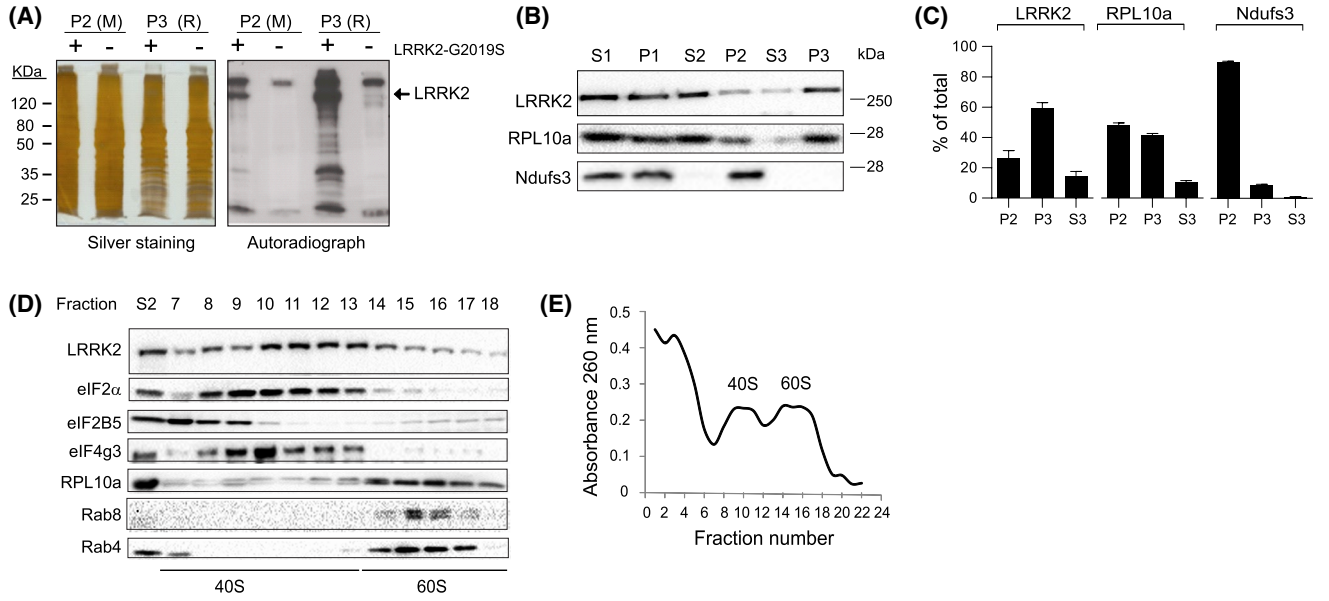

FIGURE 1 LRRK2 localizes to the 40S ribosomal subunit and phosphorylates ribosomal fractions. A, Mitochondrial (P2 (M)) and ribosomal (P3 (R)) fractions from rat brain were phosphorylated ± LRRK2-G2019S in the presence of [γ-32P]-ATP. Silver stained gels and corresponding autoradiographs of phosphorylated fractions are shown. B, Representative immunoblots of rat brain fractions probed with antibodies against LRRK2 and Ndufs3 or RPL10a, to identify mitochondria and ribosomes respectively. C, Quantitative analysis shows relative levels of markers in P2, P3, and S3, expressed as % of total (P2+P3+S3 combined). Mean values ± standard error of the mean SEM from four independent repeats are shown. D, Post-mitochondrial supernatant (S2) was separated on 5%-50% sucrose gradient and fractions were immunoblotted for ribosomal (eIF2α, eIF2B5, eIF4g3, and RPL10a) and endosomal (Rab4, Rab8) markers, as indicated. LRRK2 was enriched at the 40S ribosomal subunit. E, The absorbance at 260 nm for ribosomal fractions shown in D indicates fractions with 40S and 60S ribosomes

function in neurons. Specifically we examined the effect of three structurally independent LRRK2 inhibitors (IN1, GSK-2578215A, and MLi-2),[41-43] on de novo protein synthesis using noncanonical amino acid labeling as previously.[31,44] We labeled neurons with the Met-analog L-AHA, followed by cycloaddition of Alexa-488. Treatment for 1 hour with any one of these three inhibitors increased protein synthesis in cultured dopaminergic and hippocampal neurons, as measured either in the cell soma or the dendrites (Figures 2 and S2). Notably, there was a close match between doses of LRRK2 inhibitor that reduced activity of LRRK2 (visualized by reduced phosphorylation of LRRK2 on S935 and Rab10 on T73), and doses that increased translation (Figures 2A-N and S2). As previously reported,[45] we found no change in LRRK2 protein levels following 1 hour treatment with LRRK2 inhibitors (Figures 2O and S2D). As a negative control, we treated cells with anisomycin, an inhibitor of peptidyl transfer. This treatment effectively reduced translation as expected (Figure 2E-F,J).

We next checked whether LRRK2 inhibitors altered translation measured using classical $^{[35]}$S-methionine labeling. As low as 10 nM MLi-2 increased protein synthesis in neurons by 16% (Figure 3A), and anisomycin inhibited it (Figure 3B). This was compared to 50% increase using AHA, as AHA labeling is more sensitive as it measures from single cell types rather than population analysis.[31]

3.3 | Neurons from *Lrrk2*−/− mice show increased translation as do neurons after *Lrrk2* knockdown

To validate that the effect of LRRK2 inhibitors on protein synthesis were indeed due to LRRK2 inhibition, we measured protein synthesis in neurons isolated from wild-type and *Lrrk2*−/− mice. Consistent with the earlier pharmacological approaches, we found that protein synthesis was significantly increased in cultured neurons from *Lrrk2* knockout mice compared to wild-type littermates (Figure 3C,D). Notably, treatment with MLi-2 had no further effect on protein synthesis in *Lrrk2*−/− neurons (Figure 3C,D), further validating that this inhibitor effect on protein synthesis was mediated by LRRK2 inhibition rather than an off-target effect. Finally, we tested the effect of *Lrrk2* knockdown on protein synthesis. Primary hippocampal neurons were transfected with *Lrrk2* siRNA and incubated for 14 days after which endogenous LRRK2 expression reduced by 50% (Figure 3E,F). Protein synthesis showed a concomitant increase in *Lrrk2* knockdown cells (Figure 3G).

3.4 | LRRK2-G2019S inhibits translation in a cell free assay

To determine if LRRK2-G2019S acts directly on ribosomes to inhibit translation, we used an in vitro translation system

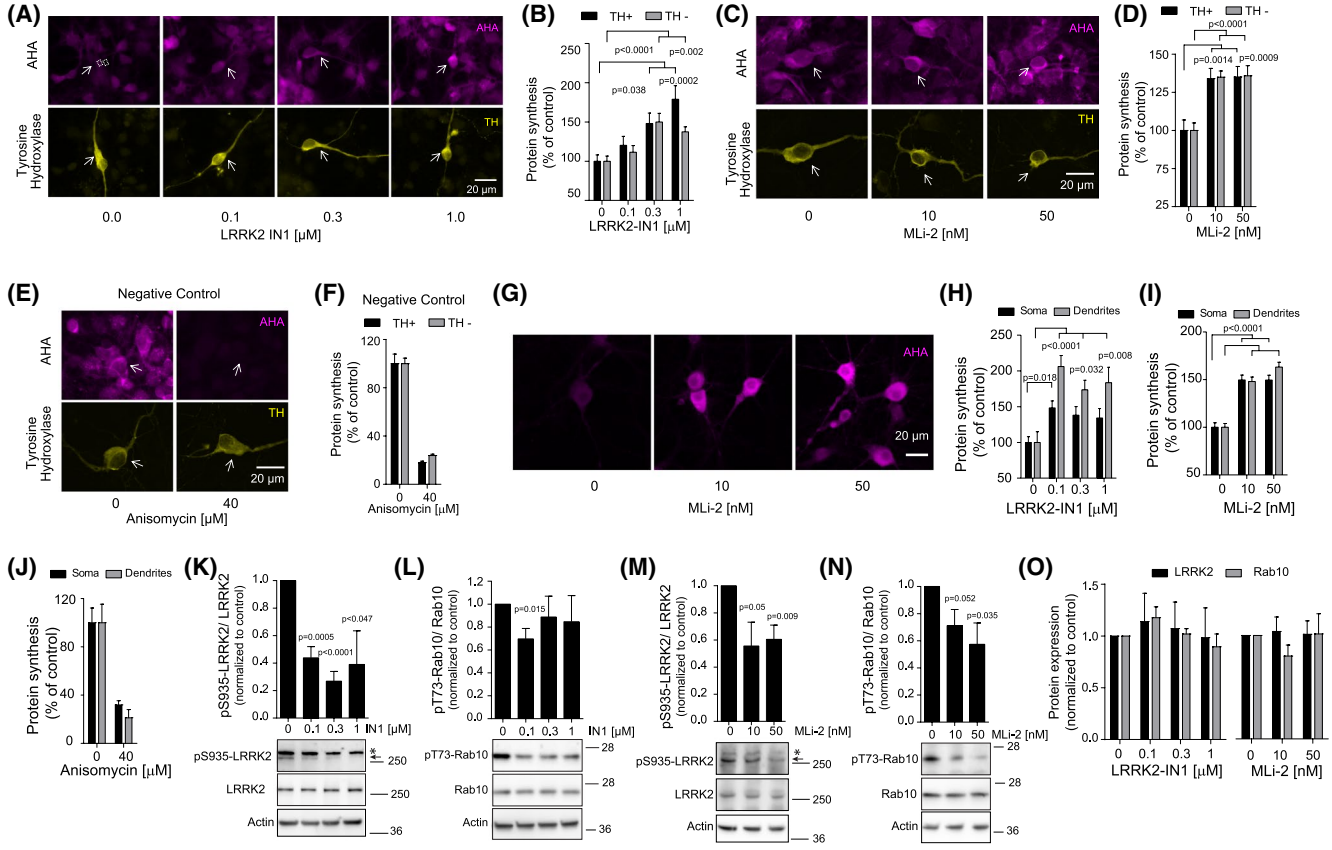

FIGURE 2 LRRK2 suppresses RNA translation in neurons. A-J, Midbrain neurons (A-F) or hippocampal neurons (G-J), were treated for 60 minutes with LRRK2 inhibitors, anisomycin or DMSO (0.1%) as indicated. De novo protein synthesis was measured from AHA-Alexa-488 (magenta) labelled cells and representative images are shown in A, C, E, and G. R.o.i. rectangles on A depict regions where soma and background intensities were measured. Mean soma intensities ± SEM of AHA-Alexa-488 fluorescence is shown from TH+ and TH− neurons (B, D, F). Data were collected from 10 to 37 neurons per condition. Significance was determined by one-way ANOVA after Bonferroni post-hoc test. G-J, In hippocampal neurons (G), mean fluorescence intensities from soma and dendrites are shown. Mean data from 15-27 cells/condition for H and J or >68 cells for I ± SEM are shown. Adjusted *P* values determined from one-way ANOVA after Bonferroni post hoc test are indicated. K-O, Hippocampal neurons treated as described (G-I), were immunoblotted with antibodies detecting p-S935-LRRK2 and LRRK2 (K,M) or p-T73-Rab10 and Rab10 (L,N), and actin. (O) Quantitative data for LRRK2 and Rab10 protein levels. Means ± SEM from four experiments are shown. *P* values were calculated using Student's *t* test. The p-S935-LRRK2 band equivalent to the R_f value of the full length LRRK2 (arrow) was quantitated. The "*" indicates a nonspecific band that is not detected by the LRRK2 antibody. Values for mw (kDa) are shown beside the gels

where purified ribosomal machinery is used to translate a β-galactosidase reporter in a cell free assay. Addition of recombinant LRRK2-G2019S reduced translation by 40% (Figure 3H). This suggests that LRRK2 directly phosphorylates components of the translational machinery to inhibit translation. To distinguish whether LRRK2 regulated regular CAP-dependent translation or IRES-regulated translation, which is important under conditions of oxidative stress,[46] we used the bi-cistronic pYIC fluorescence reporter, where CAP- and IRES-dependent translation are simultaneously measured by YFP and CFP, respectively. LRRK2 inhibitor increased both CAP and IRES-dependent translation in neurons (Figure S3). In summary, we find using four independent measuring approaches that LRRK2 activity represses protein synthesis in neurons.

3.5 | Translation is decreased in rotenone and 6-OH dopamine models of Parkinson's

We next looked for cellular models of Parkinson's to test whether translation was impaired. We used rotenone to model sporadic Parkinson's disease, as in rodents rotenone reproduces Lewy body hallmarks of sporadic Parkinson's disease,[47] and exposure evokes acute onset of Parkinson's symptoms in humans while being associated with increased risk to develop the disease.[48] Rotenone is at once a mitochondrial complex I inhibitor and a microtubule toxin.[49,50] We found that treatment of mid brain cultures with rotenone increased LRRK2 activity, as assessed by increased phosphorylation of LRRK2-S935 and of the LRRK2 substrate Rab10-T73

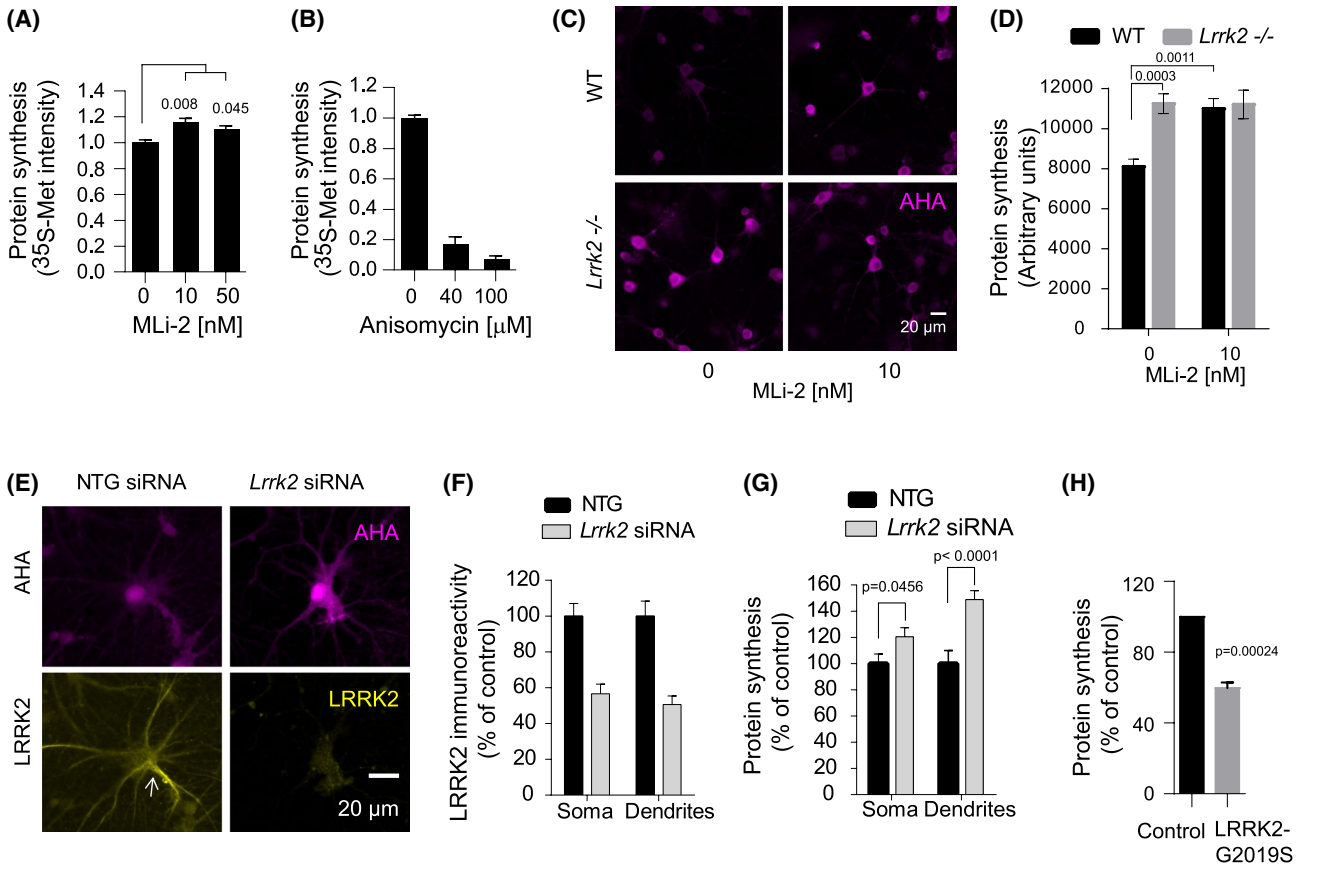

FIGURE 3 Knockdown or knockout of *Lrrk2* increases protein synthesis. A,B, Hippocampal neurons at 20 days were treated with MLi-2 or anisomycin for 90 minutes, and protein synthesis was measured using [35]S-Met labeling. Quantitative data shows [35]S-Met labeled protein intensity. Mean values ± SEM relative to control for MLi-2 (n = 4) and anisomycin (n = 3) are shown. Adjusted *P* values determined by one-way ANOVA with Bonferroni post hoc test are shown. C,D, Protein synthesis was measured using AHA-labeling in WT and *Lrrk2*−/− hippocampal neurons at 16 days in culture, ±10 nM MLi-2 for 60 minutes. Representative images are shown. Means ± SEM from 52 cells/condition are shown. Adjusted *P* values were determined using two-way ANOVA with Bonferroni corrections. E,F, Hippocampal neurons were transfected with *Lrrk2* siRNA or nontargeting (NTG) siRNA as shown. Representative images in E show relative LRRK2 expression (yellow, arrow) and AHA-Alexa-488. F, Quantitative data for LRRK2 immunoreactivity is shown. G, The effect of *Lrrk2* knockdown on protein synthesis is shown for 47-64 cells/condition. *P* values were determined using Student's *t* test. H, The effect of LRRK2-G2019S on protein synthesis in a cell-free translation system is shown (±SEM) from three experiments is shown. *P* values were determined using Student's *t* test

(Figures 4A,B and S4A). Consistent with this, rotenone reduced translation by 40% in dopaminergic neurons and this was prevented by LRRK2 inhibitor MLi-2 (Figure 4C). The same was found in 6-OH dopamine-treated dopaminergic neurons. These results indicate that protein synthesis is repressed in a LRRK2-dependent fashion in cellular models of Parkinson's disease.

3.6 | Rotenone induces dopaminergic neuron atrophy that is prevented upon LRRK2 inhibition

We next investigated whether LRRK2 activity contributed to neurite wasting or atrophy of dopaminergic neurons, a pathological feature of Parkinson's disease. As low as 1 nM of rotenone induced a substantial die back of neurites in dopaminergic neurons in culture without compromising viability (Figure 4D,E). Neurite atrophy was prevented by LRRK2 inhibitors (IN1, GSK-2578215A, or MLi-2; Figure 4E,F). To determine if atrophy was dependent on repressed translation, we measured the effect of inhibiting translation on neurite integrity. Treatment with either anisomycin or rotenone induced a similar level of neurite atrophy and there was no additional atrophy in neurons treated with anisomycin and rotenone together (Figure 4G). This shows that actually, repressing protein synthesis is sufficient to disturb neurite integrity and is consistent with our model where rotenone activates LRRK2 leading to repressed translation and compromised integrity of dopaminergic neuron processes.

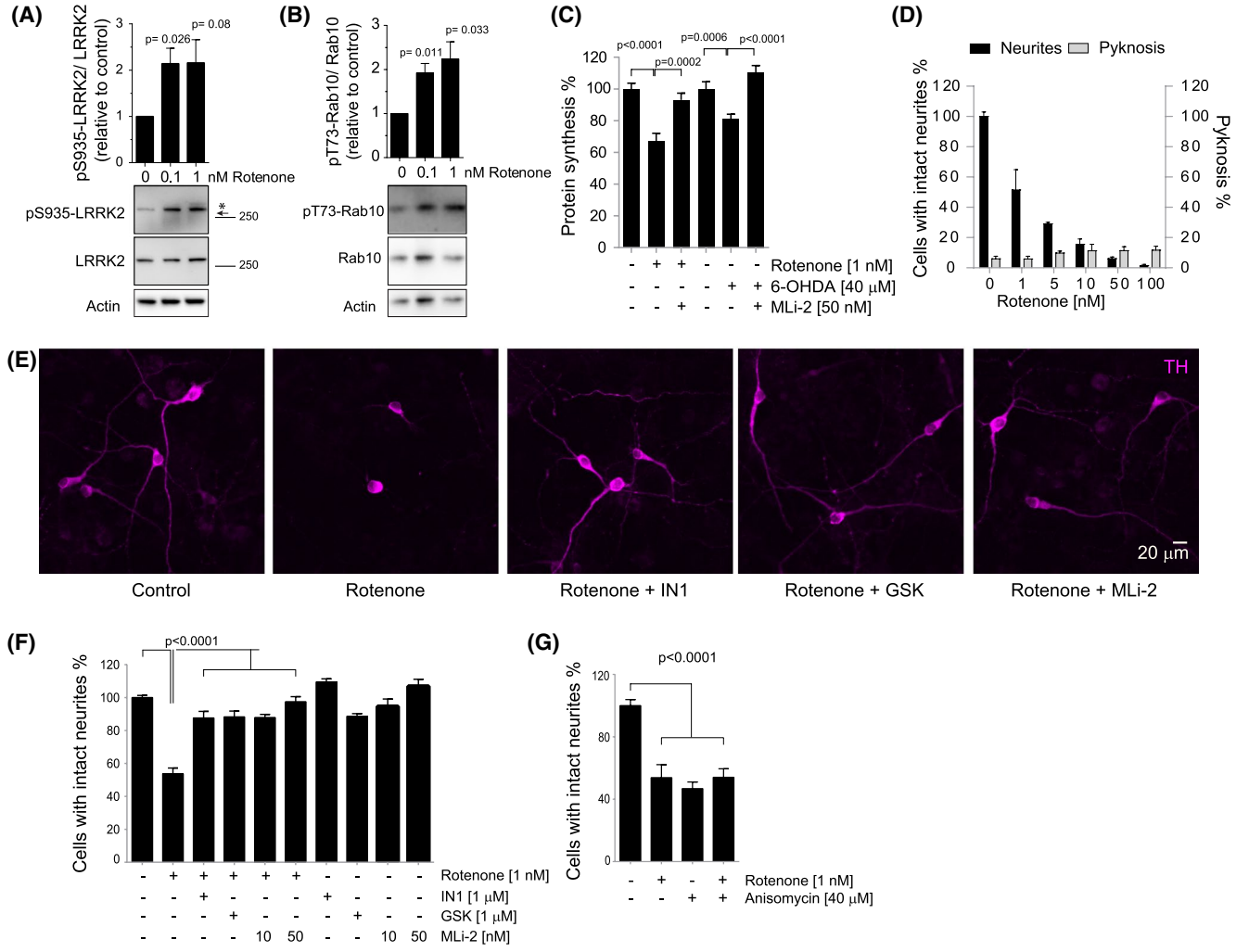

FIGURE 4 Rotenone activates LRRK2 and induces LRRK2-dependent atrophy of dopaminergic neurons. A,B, Mid brain cultures were treated with rotenone for 24 hours. Immunoblotting for p-S935-LRRK2 and LRRK2 (A) or p-T73-Rab10 and Rab10 (B), are shown. The arrowhead indicates full length LRRK2. The "*" indicates a nonspecific band that is not detected by the LRRK2 antibody. Quantitative data ± SEM is from three experiments. *P* values were from Student's *t* test. C, TH+ neurons at 3 days were treated with 1 nM rotenone or 40 μM 6-OHDA ± 50 nM MLi-2. Protein synthesis was measured after 24 hours using AHA-labeling. Mean values are from 45-61 cells/condition ± SEM *P* values from Student's *t* test are indicated. D, The proportion of TH+ neurons with intact neurites (expressed as % of control) or with pyknotic nuclei are shown following 24 hours rotenone treatment. Mean data ± standard deviations are shown from two experiments. E, Representative images from F depict TH+ immunostained neurons in magenta. F, Neurite atrophy was measured from TH+ neurons treated with 1 nM rotenone ± LRRK2-IN1 (1 μM), GSK-2578215A (1 μM) or MLi-2 (50 nM) for 24 hours. Significance was determined by one-way ANOVA and Bonferroni post-hoc test from four experiments. Adjusted *P* values are shown. G, TH+ neurons were treated with 40 μM anisomycin or 1 nM rotenone for 24 hours as indicated. The proportion of cells with intact neurites is expressed as % of control. Mean values ± SEM are indicated. Adjusted *P* values are from one-way ANOVA and post hoc Bonferroni, from four experiments

3.7 | LRRK2 acts downstream of mitochondria to repress translation

As rotenone inhibits mitochondrial complex I leading to increased oxidative damage,[51] we tested whether the effect of LRRK2 on translation and atrophy could be a consequence of ATP depletion. Rotenone reduced neuronal ATP levels in a dose-dependent manner, consistent with complex I inhibition (Figure S4B,C). However, this was not prevented upon treatment with LRRK2 inhibitor, indicating that LRRK2 action is either downstream of mitochondrial dysfunction or acting on an independent mechanism. Thus, impaired translation, which is rescued by LRRK2 inhibitors, is unlikely to be a consequence of ATP depletion.

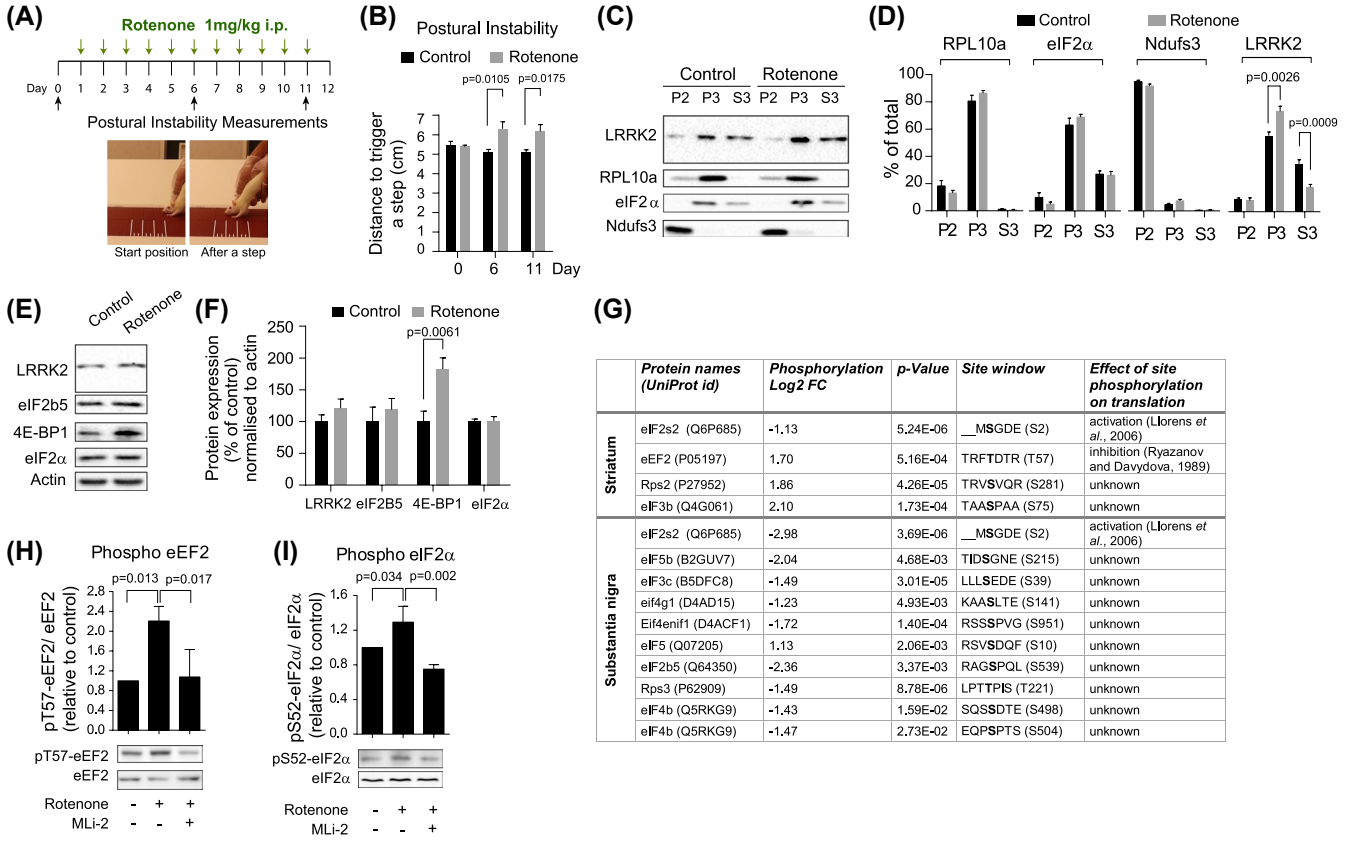

	Protein names (UniProt id)	Phosphorylation Log2 FC	p-Value	Site window	Effect of site phosphorylation on translation
Striatum	eIF2s2 (Q6P685)	-1.13	5.24E-06	__MSGDE (S2)	activation (Llorens *et al.*, 2006)
	eEF2 (P05197)	1.70	5.16E-04	TRFTDTR (T57)	inhibition (Ryazanov and Davydova, 1989)
	Rps2 (P27952)	1.86	4.26E-05	TRVSVQR (S281)	unknown
	eIF3b (Q4G061)	2.10	1.73E-04	TAASPAA (S75)	unknown
Substantia nigra	eIF2s2 (Q6P685)	-2.98	3.69E-06	__MSGDE (S2)	activation (Llorens *et al.*, 2006)
	eIF5b (B2GUV7)	-2.04	4.68E-03	TIDSGNE (S215)	unknown
	eIF3c (B5DFC8)	-1.49	3.01E-05	LLLSEDE (S39)	unknown
	eif4g1 (D4AD15)	-1.23	4.93E-03	KAASLTE (S141)	unknown
	Eif4enif1 (D4ACF1)	-1.72	1.40E-04	RSSSPVG (S951)	unknown
	eIF5 (Q07205)	1.13	2.06E-03	RSVSDQF (S10)	unknown
	eIF2b5 (Q64350)	-2.36	3.37E-03	RAGSPQL (S539)	unknown
	Rps3 (P62909)	-1.49	8.78E-06	LPTTPIS (T221)	unknown
	eIF4b (Q5RKG9)	-1.43	1.59E-02	SQSSDTE (S498)	unknown
	eIF4b (Q5RKG9)	-1.47	2.73E-02	EQPSPTS (S504)	unknown

FIGURE 5 Rotenone regulates phosphorylation of protein synthesis checkpoints. A, Experimental timeline and snapshots of rats undergoing postural instability test. B, Rats were treated with rotenone or vehicle and postural instability was tested from six animals per condition. Distance to trigger a step is shown. *P* values were determined using Student's *t* test. C,D, Brain fractions from rats after behavioral testing were immunoblotted for ribosomal or mitochondrial markers and for LRRK2. Relative protein levels in P2 (mitochondrial pellet), P3 (ribosomal pellet), and S3 are shown. LRRK2 accumulated at the ribosomal fraction in rotenone-treated rats. Significance was determined using Student's *t* test. E, Immunoblots of brain homogenates from rotenone treated. F, Quantitative data from six animals per condition of blots as shown in E. Mean values ± SEM are shown. Significance was determined using Student's *t* test. G, Mass spectrometry analysis of phosphoproteins in substantia nigra and striatum of control (n = 12) and rotenone treated (n = 14) rats was carried out. Several of the significantly changing phosphoproteins were ribosomal-associated. Phosphorylation fold change (FC) is shown as Log2 scale. *P* values (Student's *t* test) are indicated. FDR was <0.05. Aforementioned parameters, as well as protein names, UniProt identifiers and assigned sites are shown. The site window for each phosphosite is indicated with the phosphorylated residue bolded, and effect of phosphorylation on that site is described. H, I, Midbrain cultures were treated with DMSO or 1 nM rotenone ∓ 10 nM MLi-2 for 24 hours and lysates were immunoblotted for pT57-eEF2 and eEF2 (H) or pS52-eIF2α and eIF2α (I). Mean data ± SEM from three experiments is shown. Significance was determined by one-way ANOVA and Bonferroni post-hoc test

3.8 | Checkpoint regulators of protein synthesis arrest are switched on in the rotenone model

We next tested rotenone in vivo in rats (Figure 5A,B). After behavioral testing, brains were extracted and ribosomal fractions were analyzed as earlier (Figure 1B). Ribosomal and mitochondrial fractions were validated using specific markers; RPL10a for the 60S ribosomal subunit, eIF2α for the 40S subunit and Ndufs3 as a mitochondrial marker (Figure 5C,D). Interestingly, LRRK2 was enriched in the ribosomal fractions from rotenone treated rats with a concomitant decrease in the remaining supernatant (Figure 5D). Also notable, expression of the translation repressor 4E-BP1 was increased in brains from rats treated with rotenone (Figures 5E,F and S5A). These changes indicate that translation is repressed in brain of rotenone-treated rats.

We performed a mass spectrometry-based analysis of protein phosphorylation changes in substantia nigra and striatum of control and rotenone-treated rats. This revealed that highly significant phosphorylation changes occurred to regulators of translation initiation and elongation (Figure 5G). Specifically, in striatum, eIF2s2-S2 (eIF2β), eEF2-T57, eIF3b, and RPS2 phosphorylation was significantly altered. Similarly, eIF2s2-S2, eIF5b, eIF3c, eIF4G1, eIF4E transporter, eIF5, eIF2b5, eIF4b, and RPS3 phosphorylation was significantly altered in the substantia nigra. Among these, phosphorylation of eIF2s2 (eIF2β) was decreased on S2 in both regions. eIF2s2 is a part of the trimeric eukaryotic initiation factor 2 (eIF2) complex, that recruits Met-tRNAi as a rate-limiting

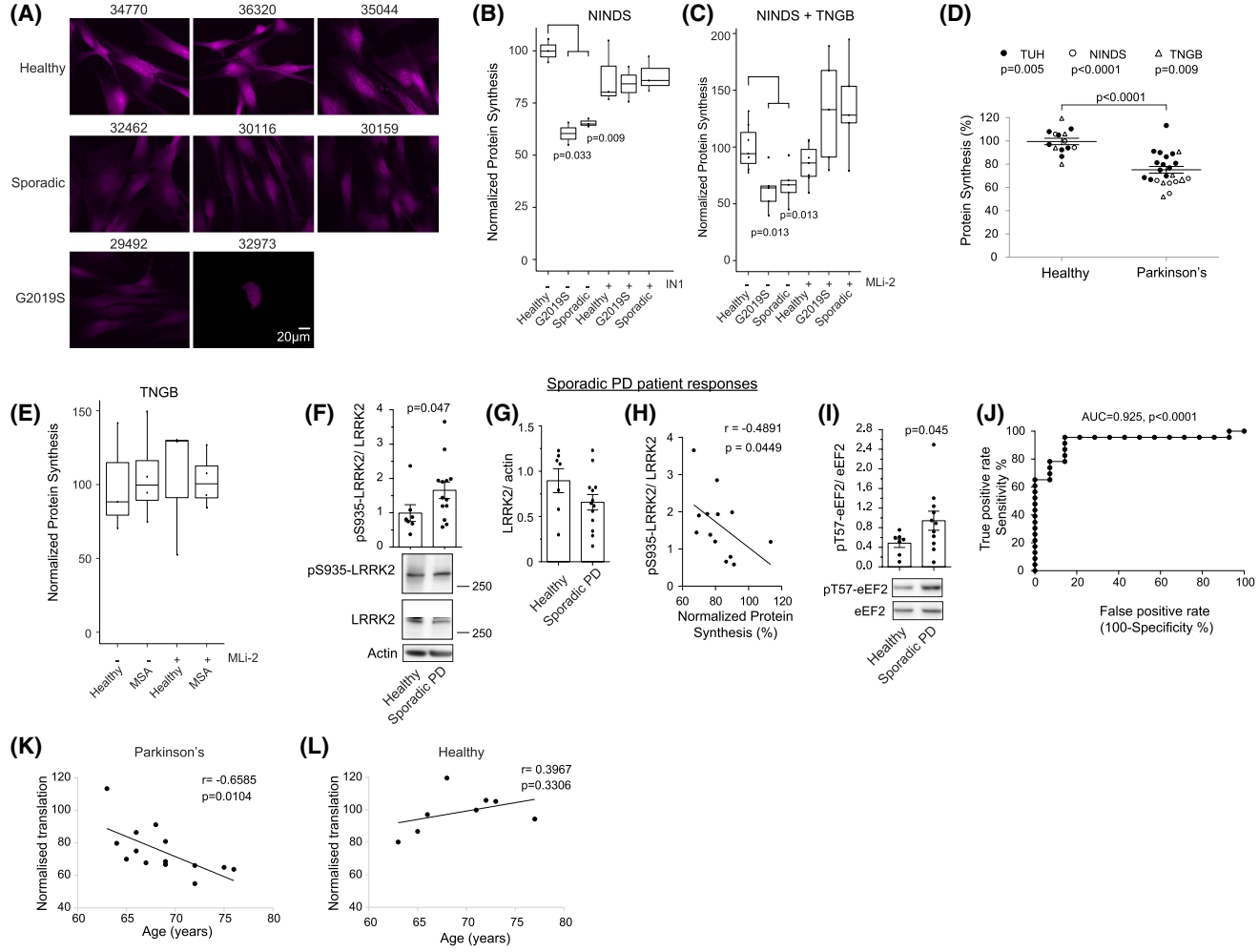

FIGURE 6 Protein synthesis is reduced in skin fibroblasts from sporadic and G2019S Parkinson's patients. All patient demographics are in Table S1. A, Representative images of AHA-labeled skin cells from sporadic or G2019S Parkinson's patients or from healthy controls are shown. NINDS repository numbers are below the panels. B, Quantitative protein synthesis data from healthy, sporadic or G2019S cases ± LRRK2-IN1 (1 μM) treatment are plotted. Adjusted *P* values were calculated using *t* test followed by Benjamini and Hochberg testing. C, Protein synthesis measured as in B, but with MLi-2 (100 nM) inhibitor. Combined data for samples from NINDs repository, Telethon Network of Genetic Biobanks (TNGB) are shown. D, Cells were isolated from skin biopsies from early stage Parkinson's patients or healthy volunteers at Turku University Hospital (TUH). Protein synthesis is expressed as mean data ± SEM Significance was determined using Student's *t* test. E, Protein synthesis data from fibroblasts from Multiple System Atrophy (MSA) patients (n = 4) or healthy individuals (n = 3). F, G, Cell lysates from sporadic cases were immunoblotted for pS935-LRRK2, total LRRK2, and actin. Mean data shows LRRK2 activity or LRRK2 levels ± SEM. Significance was determined using Student's *t* test. H, The correlation between protein synthesis and phospho-S935 LRRK2 is shown from patient cells. Pearson's coefficient (*r*) and the *P* value are indicated on the graph. I, Lysates from F were immunoblotted for pT57-eEF2 and eEF2. Significance was determined using Student's *t* test. J, The receiver operating characteristic (ROC) curve for protein synthesis measured from all patient samples (TUH, NINDS and TNGB) is shown. Area under the curve (AUC) was 92.5%. *P* value was determined with Student's *t* test. K, L, Correlation of translation and patient age is shown for patients >60 years. A significant correlation was found between repression of translation and increased age in patients but not in healthy controls

step during translation initiation. Loss of phosphorylation on S2 prevents translation.[52] Moreover, phosphorylation of eEF2-T57 was increased. eEF2 translocates nascent peptidyl-tRNAs during elongation. Phosphorylation on T57 inactivates eEF2, thereby reducing elongation.[53-56] These phosphorylation changes represent critical checkpoint steps during translation. The phosphorylation changes observed on these sites indicate that protein synthesis is repressed in the striatum and substantia nigra of rotenone-treated rats.

We next examined if phosphorylation of translation checkpoint regulators was LRRK2 dependent. Using a phospho-specific antibody against eEF2-T57, we found that rotenone induced phosphorylation of this site was prevented by treatment with LRRK2 inhibitor MLi-2 (Figure 5H). We also

tested phosphorylation of the eIF2 complex on eIF2α–S52, as phosphorylation of this site marks another rate limiting step during translation.[57] Rotenone increased eIF2α–S52 phosphorylation, indicating protein synthesis arrest, and this was prevented by treatment with MLi-2 (Figures 5I and S5B). These data identify that LRRK2 activity induces phosphorylation changes to checkpoint regulators of translation that signal protein synthesis arrest.

3.9 | Protein synthesis is reduced in skin cells from sporadic and G2019S Parkinson's subjects compared to healthy, age-matched individuals

LRRK2 is widely expressed among tissues and by no means confined to brain. We therefore decided to test whether translation was impaired in skin cells from Parkinson's subjects. We started by measuring translation in skin fibroblasts from Parkinson's patients and healthy individuals as these have been used to aid mechanistic understanding.[58] We obtained from the National Institute of Neurological Disorders (NINDS) repository and from the Telethon Network of Genetics Biobanks (TNGB). Patient demographics, including age, sex, UPDRS, and Hoehn & Yahr stage, as well as [^{123}I]FP-CIT-SPECT data for striatal dopamine transporter binding are described in Table S1. Global protein synthesis was reduced by 40% or greater in cells from sporadic and G2019S patients (Figure 6A-C). This was reversed upon treatment with LRRK2 inhibitors (Figure 6B,C), indicating that LRRK2 activity was responsible for reduced protein synthesis not only in G2019S cases, but also in sporadic subjects. To validate these results, we collected additional skin punches from 13 sporadic Parkinson's patients attending Turku University Hospital (TUH) in Finland and 7, age matched controls. Patients were not fully diagnosed at the time of sampling, but all progressed to have a clinical diagnosis of Parkinson's disease within 24 months using UK Brain Bank criteria.[59] Global protein synthesis was reduced in this TUH patient group, when analyzed alone ($P = .005$, size effect = 1.56, power = 0.88; Figure 6D, black circles) or when combined with NINDS and TNGB cohorts ($P < .0001$, size effect = 1.91, power = 0.99; Figure 6D). These data indicate that repressed protein synthesis provides a specific biomarker readout of Parkinson's disease from patient cells even at an early stage.

3.10 | Protein synthesis is unchanged in cells from multiple system atrophy patients

Atypical Parkinsonian disorders are mechanistically distinct from Parkinson's disease but show overlapping symptoms so are difficult to distinguish. Interestingly, we found no evidence that protein synthesis was repressed in MSA patient cells (Figure 6E). Nor did we find a difference in cells from a patient with progressive supranuclear palsy (data not shown), suggesting that translation deregulation may be specific to Parkinson's disease.

3.11 | LRRK2-S935 phosphorylation correlates with repressed translation in cells from sporadic patients

We next examined whether LRRK2 was activated in skin cells from sporadic patients. LRRK2-S935 phosphorylation increased by 50% in patient cells compared to healthy donors (Figure 6F,G). Moreover, there was a correlation between LRRK2-S935 phosphorylation and repressed protein synthesis, consistent with LRRK2 being responsible (Figure 6H). Also, the elongation checkpoint marker, eEF2-T57 phosphorylation was increased in sporadic patient cells (Figure 6I), once more indicating repressed translation. Finally, the ROC curve for patient translation data indicated that this measurement provides good predictive power from patient skin cells (Figure 6J).

3.12 | Repression of translation correlates with age in Parkinson's patients

As age is a major predisposing factor to develop Parkinson's disease, we measured whether the reduced overall translation response in Parkinson's patients increased as these patients aged. We found that there was a negative correlation between translation and patient age in individuals older than 60 years (Pearson's coefficient = −0.6585, $P = .01$), but not in younger patients (Figures 6K,L, and S6). Thus, translation became progressively more inhibited in Parkinson's patients after 60 years of age (Figure 6K), whereas protein synthesis did not decline in the same way in otherwise healthy, aging individuals (Figure S6). This fits with the theory that Parkinson's disease is an accelerated form of aging, and suggests that reduced translation in Parkinson's disease may represent accelerated aging.

In summary, our data show that LRRK2 is activated in cells from sporadic patients leading to an overall reduction in translation. Measurement of this protein synthesis deficit may provide a means to distinguish between healthy and Parkinson's individuals.

4 | DISCUSSION

In this study, we show that LRRK2 represses protein synthesis in animal models of sporadic Parkinson's disease and in

fibroblasts from sporadic and LRRK2-G2019S patients. We use pharmacological inhibition of LRRK2, gene silencing and genetic deletion of *Lrrk2* to demonstrate that repression of protein synthesis is LRRK2-dependent. We identify that known checkpoint regulators of translation are phosphorylated on sites that signal protein synthesis arrest, in animal models and patient cells. Our findings suggest that LRRK2 exerts a repressive regulation of protein synthesis and that this may be a proximal action of LRRK in Parkinson's disease pathology.

Here, we use the rotenone model of Parkinson's disease as it replicates pathological hallmarks of the sporadic form such as Lewy bodies, postural instability and behavioral deficits that are reversed by L-DOPA.[34,47,51,60] Also, exposure to rotenone, a naturally occurring insecticide used in farming, is associated with increased Parkinson's risk,[48] making it a relevant model for sporadic Parkinson's disease, along with the more commonly used 6-hydroxy dopamine model.[61] In both models, we find that LRRK2 is activated and reduces protein synthesis while also inducing atrophy of dopaminergic neurites, an early event in the disease pathology.[62] Indeed, we show that merely inhibiting protein synthesis using anisomycin induces dopaminergic neuron atrophy and rotenone has no further effect. This indicates that neurite homeostasis and de novo protein synthesis are tightly coupled in dopaminergic neurons and that repression of protein synthesis alone could explain the extent of atrophy obtained with rotenone and 6-hydroxy dopamine.[63]

The possibility that LRRK2 may regulate translation has generated interest for some years.[18-20,64] LRRK2 interacts with translational machinery; eIF2C1, EIF2C2, and bifunctional amino-acyl tRNA synthase.[17] Also, *EIF2* signaling is severely disrupted in blood from sporadic and G2019S patients alike.[65] While these data imply that LRRK2 regulates ribosomal function, direct measurement of translation in mammalian models of Parkinson's disease or in patient cells, using methods that do not themselves disturb protein homeostasis, have been lacking. Here, we use several methods to measure the effect of LRRK2 on RNA translation. For example, we do two types of metabolic labeling, using either a methionine analog (AHA), or a methionine isotope (^{35}S-Met). Both approaches avoid overexpression. We also measure in vitro translation directly in a reconstituted system. Finally, we use a gene reporter to monitor translation in models of sporadic Parkinson's disease and in patient cells. We find consistently that translation is repressed by LRRK2 irrespective of the method or disease model used, rotenone and 6-hydroxydopamine models yielding equivalent results.

In contrast to our findings in mammalian cells, human LRRK2-G2019S overexpression in *Drosophila* was shown to increase translation compared to endogenous wild-type *Drosophila* LRRK2.[20] This difference may be explained by contextual differences. For example, although human LRRK2-G2019S was expressed in *Drosophila*, it was compared to endogenous *Drosophila* LRRK2 which diverges substantially (16% sequence match) from human LRRK2, and even misses part of the kinase domain.[66] Moreover, *Drosophila* ribosomal proteins show poor sequence homology with human, whereas rat ribosomal proteins are 99% identical to human,[67,68] making rat a more suitable model. Lastly, some of the data showing increased translation used reporter overexpression to track protein synthesis.[20,64] Such overexpression overloads cellular resources in particular translational machinery, leading to disturbed homeostasis of cellular machinery and can even trigger promiscuous signaling.[69,70] For this reason, we avoided reliance on overexpression, and rather used amino acid labeling to measure translation. Overall, it is not too surprising that the effect on translation obtained in *Drosophila* models differs from our data in mouse, rat, and human cells. It is particularly significant that we find the same effect with endogenous human LRRK2 and human G2019S-LRRK2 in their natural cellular environment, that is, patient skin cells.

We find that rotenone increases phosphorylation of eIF2α (S52) on a site that inhibits translation at the initiation stage.[52,57] Specifically, phosphorylation of eIF2α (S52) blocks $tRNA^{Met}$ association with the 40S ribosomal subunit, thereby suppressing translation.[71-73] Interestingly, increased phosphorylation of eIF2α (S52) is also found in the substantia nigra of Parkinson's patients,[21] and *eiF2α* mRNA is dysregulated.[21,65] We also find that 4E-BP1 is increased by rotenone. This will also inhibit translation by sequestration of eIF4E.[74,75] Finally, we find that eEF2-T57 phosphorylation is increased. This will inhibit its recruitment to ribosomes and stall elongation.[53-56] We know from other neurological diseases that disturbed translation causes neurodegeneration, for example, in childhood ataxia, where eIF2B5 is mutated.[76,77] In summary, several checkpoints of protein synthesis arrest are switched on in the substantia nigra and striatum of rotenone-treated rats, in rotenone treated dopaminergic neurons and in patient cells. While these phosphorylation changes are not necessarily directly executed by LRRK2, they would appear to be dependent on LRRK2 as they are prevented when LRRK2 is inhibited, suggesting that LRRK2 triggers protein synthesis arrest via these downstream events.

SNpc dopaminergic neurons are particularly vulnerable in Parkinson's disease, raising the next question; whether this vulnerability could be explained by a greater dependence on de novo protein synthesis in these cells. SNpc dopaminergic neurons host an exceptionally high density of ribosomes compared to neighboring cells, and are thus equipped for elevated protein synthesis.[78,79] This has been attributed to the need for these cells to facilitate large-scale synthesis of antioxidant proteins that are required to counteract the reactive oxygen species generated from dopamine metabolism.[80] This would make them particularly vulnerable to repressed protein

synthesis. On the contrary, slowing of protein synthesis was shown to preserve the fidelity of RNA decoding and facilitate protein folding, and oxidative stress can itself reduce the speed of translation.[81] Thus, the physiological function of LRRK2 may be to facilitate this quality control whereas. Under pathological conditions, hyper-activation of LRRK2 over a longtime period may lead to excessive slowing and run-down in expression of critical proteins, such as those required for protein folding. One can even envisage how this could contribute to α-synuclein oligomer formation, a pathological hallmark in both sporadic and LRRK2-G2019S PD.

We demonstrate that LRRK2 is activated and translation is reduced in peripheral cells from patients. While we think this mechanism of LRRK2 is common to all areas where it is expressed, including brain, it raises a question concerning the non-motor symptoms of Parkinson's disease that occur in the periphery such as olfactory, gastrointestinal, respiratory, skin, sleep, visual, and neuropsychiatric dysfunction.[2] One could speculate that LRRK2 may contribute for example to disease-associated skin problems, for example, seborrhea and hypo/hyperhidrosis. Moreover, α-synuclein aggregates also appear in patient skin,[82] a possible consequence of stalled translation. Moreover, prodromal symptoms of depression and anxiety are already associated with deregulated protein synthesis,[83-85] and impaired translation has been factored in sleep disorders.[84] Thus, repression of translation by LRRK2 could conceivably contribute to a range of early symptoms.

Of clinical relevance, we find that repression of translation correlates with age in Parkinson's patients above 60 years, but we detect no decline in translation with aging in healthy individuals during this time-span. This is consistent with age being the greatest risk factor for Parkinson's disease and the idea that Parkinson's is a disease of accelerated aging.[86] Finally, there is a need for a Parkinson's biomarker.[87,88] Measuring translation from peripheral cells could potentially lead to a biomarker readout. While skin cells are more accessible than cerebral spinal fluid for example, it would also be of interest to examine whether the same mechanism is at play in blood cells. In summary, we identify LRRK2-dependent protein synthesis deficiency in cells from familial and sporadic Parkinson's disease and in rodent models. Measuring this deficit in peripheral cells from patients shows potential application as a biomarker readout for patient screening and diagnosis.

ACKNOWLEDGMENTS

We thank Susanna Pyökäri, Terhi Hiltula-Maisala, Benjamin Hackl, and Lassi Lauren for technical assistance and the Arumäe lab for teaching midbrain cultures. This work was funded by Turku Graduate School of Biomedical Sciences (PD), Business Finland project # 1817/31/2015 (PD, PJ, DF, and YH), Åbo Akademi University (E.C), and the Michael J. Fox Foundation (PD) and the MATTI graduate school. We acknowledge CIC, Turku Proteomics Facility and Biocenter Finland for infrastructure support.

CONFLICT OF INTEREST

The authors declare no conflict of interest

FINANCIAL DISCLOSURES

There are no financial disclosures.

AUTHOR CONTRIBUTIONS

E.T. Coffey, P. Deshpande, D. Flinkman, and V. Kaasinen contributed to conception. E.T. Coffey, P. Deshpande, D. Flinkman, Y. Hong, P. James, and L. Elo contributed to organization, design, and statistical analysis. E.T. Coffey, P. Deshpande, D. Flinkman, Y. Hong, E. Goltseva, V. Siino, L. Sun, S. Peltonen, and V. Kaasinen to execution, review, and first draft. All authors provided critique.

REFERENCES

1. Dorsey ER, Constantinescu R, Thompson JP, et al. Projected number of people with Parkinson disease in the most populous nations, 2005 through 2030. *Neurology*. 2007;68:384-386.
2. Kalia LV, Lang AE, Hazrati LN, et al. Clinical correlations with Lewy body pathology in LRRK2-related Parkinson disease. *JAMA Neurol*. 2015;72:100-105.
3. Chang D, Nalls MA, Hallgrímsdóttir IB, et al. A meta-analysis of genome-wide association studies identifies 17 new Parkinson's disease risk loci. *Nat Genet*. 2017;49:1511-1516.
4. Lesage S, Anheim M, Condroyer C, et al. Large-scale screening of the Gaucher's disease-related glucocerebrosidase gene in Europeans with Parkinson's disease. *Hum Mol Genet*. 2011;20:202-210.
5. West AB, Moore DJ, Biskup S, et al. Parkinson's disease-associated mutations in leucine-rich repeat kinase 2 augment kinase activity. *Proc Natl Acad Sci U S A*. 2005;102:16842-16847.
6. Greggio E, Jain S, Kingsbury A, et al. Kinase activity is required for the toxic effects of mutant LRRK2/dardarin. *Neurobiol Dis*. 2006;23:329-341.
7. Gilsbach BK, Kortholt A. Structural biology of the LRRK2 GTPase and kinase domains: implications for regulation. *Front Mol Neurosci*. 2014;7:32.
8. Langston RG, Rudenko IN, Cookson MR. The function of orthologues of the human Parkinson's disease gene LRRK2 across species: implications for disease modelling in preclinical research. *Biochem J*. 2016;473:221-232.
9. Healy DG, Falchi M, O'Sullivan SS, et al. Phenotype, genotype, and worldwide genetic penetrance of LRRK2-associated Parkinson's disease: a case-control study. *Lancet Neurol*. 2008;7:583-590.
10. Hulihan MM, Ishihara-Paul L, Kachergus J, et al. LRRK2 Gly2019Ser penetrance in Arab-Berber patients from Tunisia: a case-control genetic study. *Lancet Neurol*. 2008;7:591-594.
11. Haugarvoll K, Wszolek ZK. Clinical features of LRRK2 parkinsonism. *Parkinsonism Relat Disord*. 2009;15(Suppl. 3):S205-S208.
12. Di Maio R, Hoffman EK, Rocha EM, et al. LRRK2 activation in idiopathic Parkinson's disease. *Sci Transl Med*. 2018;10:eaar5429.
13. Vidyadhara DJ, Lee JE, Chandra SS. Role of the endolysosomal system in Parkinson's disease. *J Neurochem*. 2019;150:487-506.

14. Albanese F, Novello S, Morari M. Autophagy and LRRK2 in the aging brain. *Front Neurosci*. 2019;13:1352.
15. Zhao Y, Perera G, Takahashi-Fujigasaki J, et al. Reduced LRRK2 in association with retromer dysfunction in post-mortem brain tissue from LRRK2 mutation carriers. *Brain*. 2018;141:486-495.
16. Steger M, Tonelli F, Ito G, et al. Phosphoproteomics reveals that Parkinson's disease kinase LRRK2 regulates a subset of Rab GTPases. *eLife*. 2016;5:e12813.
17. Dächsel JC, Taylor JP, Mok SS, et al. Identification of potential protein interactors of Lrrk2. *Parkinsonism Relat Disord*. 2007;13:382-385.
18. Imai Y, Gehrke S, Wang HQ, et al. Phosphorylation of 4E-BP by LRRK2 affects the maintenance of dopaminergic neurons in Drosophila. *EMBO J*. 2008;27:2432-2443.
19. Gehrke S, Imai Y, Sokol N, Lu B. Pathogenic LRRK2 negatively regulates microRNA-mediated translational repression. *Nature*. 2010;466:637-641.
20. Martin I, Kim JW, Lee BD, et al. Ribosomal protein s15 phosphorylation mediates LRRK2 neurodegeneration in Parkinson's disease. *Cell*. 2014;157:472-485.
21. Hoozemans JJ, van Haastert ES, Eikelenboom P, de Vos RA, Rozemuller JM, Scheper W. Activation of the unfolded protein response in Parkinson's disease. *Biochem Biophys Res Commun*. 2007;354:707-711.
22. Jan A, Jansonius B, Delaidelli A, et al. Activity of translation regulator eukaryotic elongation factor-2 kinase is increased in Parkinson disease brain and its inhibition reduces alpha synuclein toxicity. *Acta Neuropathol Commun*. 2018;6:54.
23. Mora M, Angelini C, Bignami F, et al. The EuroBioBank Network: 10 years of hands-on experience of collaborative, transnational biobanking for rare diseases. *Eur J Hum Genet*. 2015;23:1116-1123.
24. Baptista MA, Dave KD, Sheth NP, et al. A strategy for the generation, characterization and distribution of animal models by The Michael J. Fox Foundation for Parkinson's Research. *Dis Model Mech*. 2013;6:1316-1324.
25. Nie M, Htun H. Different modes and potencies of translational repression by sequence-specific RNA-protein interaction at the 5'-UTR. *Nucleic Acids Res*. 2006;34:5528-5540.
26. Zhao Y, Spigolon G, Bonny C, Culman J, Vercelli A, Herdegen T. The JNK inhibitor D-JNKI-1 blocks apoptotic JNK signaling in brain mitochondria. *Mol Cell Neurosci*. 2012;49:300-310.
27. Björkblom B, Ostman N, Hongisto V, et al. Constitutively active cytoplasmic c-Jun N-terminal kinase 1 is a dominant regulator of dendritic architecture: role of microtubule-associated protein 2 as an effector. *J Neurosci*. 2005;25:6350-6361.
28. Hollos P, John JM, Lehtonen JV, Coffey ET. Optogenetic control of spine-head JNK reveals a role in dendritic spine regression. *eNeuro*. 2020;7. https://doi.org/10.1523/ENEURO.0303-19.2019
29. Padzik A, Deshpande P, Hollos P, et al. KIF5C S176 phosphorylation regulates microtubule binding and transport efficiency in mammalian neurons. *Front Cell Neurosci*. 2016;10:57.
30. Yu LY, Arumäe U. Survival assay of transiently transfected dopaminergic neurons. *J Neurosci Methods*. 2008;169:8-15.
31. Dieterich DC, Hodas JJ, Gouzer G, et al. In situ visualization and dynamics of newly synthesized proteins in rat hippocampal neurons. *Nat Neurosci*. 2010;13:897-905.
32. Hongisto V, Vainio JC, Thompson R, Courtney MJ, Coffey ET. The Wnt pool of glycogen synthase kinase 3beta is critical for trophic-deprivation-induced neuronal death. *Mol Cell Biol*. 2008;28:1515-1527.
33. Piccoli G, Condliffe SB, Bauer M, et al. LRRK2 controls synaptic vesicle storage and mobilization within the recycling pool. *J Neurosci*. 2011;31:2225-2237.
34. Cannon JR, Tapias V, Na HM, Honick AS, Drolet RE, Greenamyre JT. A highly reproducible rotenone model of Parkinson's disease. *Neurobiol Dis*. 2009;34:279-290.
35. Salvatore MF, Pruett BS, Dempsey C, Fields V. Comprehensive profiling of dopamine regulation in substantia nigra and ventral tegmental area. *J Vis Exp*. 2012;66:e4171.
36. Paxinos G, Watson C. *The Rat Brain in Stereotaxic Coordinates*. London: Academic Press; 2007.
37. Cox J, Mann M. MaxQuant enables high peptide identification rates, individualized p.p.b.-range mass accuracies and proteome-wide protein quantification. *Nat Biotechnol*. 2008;26:1367-1372.
38. Tyanova S, Temu T, Sinitcyn P, et al. The Perseus computational platform for comprehensive analysis of (prote)omics data. *Nat Methods*. 2016;13:731-740.
39. Ressa A, Fitzpatrick M, van den Toorn H, Heck AJR, Altelaar M. PaDuA: a python library for high-throughput (phospho)proteomics data analysis. *J Proteome Res*. 2019;18:576-584.
40. Stewart JD, Cowan JL, Perry LS, Coldwell MJ, Proud CG. ABC50 mutants modify translation start codon selection. *Biochem J*. 2015;467:217-229.
41. Deng X, Dzamko N, Prescott A, et al. Characterization of a selective inhibitor of the Parkinson's disease kinase LRRK2. *Nat Chem Biol*. 2011;7:203-205.
42. Reith AD, Bamborough P, Jandu K, et al. GSK2578215A; a potent and highly selective 2-arylmethyloxy-5-substitutent-N-arylbenzamide LRRK2 kinase inhibitor. *Bioorg Med Chem Lett*. 2012;22:5625-5629.
43. Fell MJ, Mirescu C, Basu K, et al. MLi-2, a potent, selective, and centrally active compound for exploring the therapeutic potential and safety of LRRK2 kinase inhibition. *J Pharmacol Exp Ther*. 2015;355:397-409.
44. Younts TJ, Monday HR, Dudok B, et al. Presynaptic protein synthesis is required for long-term plasticity of GABA release. *Neuron*. 2016;92:479-492.
45. Lobbestael E, Civiero L, De Wit T, Taymans JM, Greggio E, Baekelandt V. Pharmacological LRRK2 kinase inhibition induces LRRK2 protein destabilization and proteasomal degradation. *Sci Rep*. 2016;6:33897.
46. Spriggs KA, Stoneley M, Bushell M, Willis AE. Re-programming of translation following cell stress allows IRES-mediated translation to predominate. *Biol Cell*. 2008;100:27-38.
47. Betarbet R, Sherer TB, MacKenzie G, Garcia-Osuna M, Panov AV, Greenamyre JT. Chronic systemic pesticide exposure reproduces features of Parkinson's disease. *Nat Neurosci*. 2000;3:1301-1306.
48. Tanner CM, Kamel F, Ross GW, et al. Rotenone, paraquat, and Parkinson's disease. *Environ Health Perspect*. 2011;119:866-872.
49. Ren Y, Liu W, Jiang H, Jiang Q, Feng J. Selective vulnerability of dopaminergic neurons to microtubule depolymerization. *J Biol Chem*. 2005;280:34105-34112.
50. Hoebeke J, Nijen GV. Quantitative turbidimetric assay for potency evaluation of colchicine-like drugs. *Life Sci*. 1975;17:591-595.
51. Sanders LH, Greenamyre JT. Oxidative damage to macromolecules in human Parkinson disease and the rotenone model. *Free Radic Biol Med*. 2013;62:111-120.

52. Llorens F, Duarri A, Sarró E, Roher N, Plana M, Itarte E. The N-terminal domain of the human eIF2beta subunit and the CK2 phosphorylation sites are required for its function. *Biochem J*. 2006;394:227-236.
53. Ryazanov AG, Shestakova EA, Natapov PG. Phosphorylation of elongation factor 2 by EF-2 kinase affects rate of translation. *Nature*. 1988;334:170-173.
54. Ovchinnikov LP, Motuz LP, Natapov PG, et al. Three phosphorylation sites in elongation factor 2. *FEBS Lett*. 1990;275:209-212.
55. Ryazanov AG, Davydova EK. Mechanism of elongation factor 2 (EF-2) inactivation upon phosphorylation. Phosphorylated EF-2 is unable to catalyze translocation. *FEBS Lett*. 1989;251:187-190.
56. Price NT, Redpath NT, Severinov KV, Campbell DG, Russell JM, Proud CG. Identification of the phosphorylation sites in elongation factor-2 from rabbit reticulocytes. *FEBS Lett*. 1991;282:253-258.
57. Kimball SR. Eukaryotic initiation factor eIF2. *Int J Biochem Cell Biol*. 1999;31:25-29.
58. Carling PJ, Mortiboys H, Green C, et al. Deep phenotyping of peripheral tissue facilitates mechanistic disease stratification in sporadic Parkinson's disease. *Prog Neurogibol*. 2020;187:101772.
59. Hughes AJ, Daniel SE, Kilford L, Lees AJ. Accuracy of clinical diagnosis of idiopathic Parkinson's disease: a clinico-pathological study of 100 cases. *J Neurol Neurosurg Psychiatry*. 1992;55:181-184.
60. Alam M, Schmidt WJ. L-DOPA reverses the hypokinetic behaviour and rigidity in rotenone-treated rats. *Behav Brain Res*. 2004;153:439-446.
61. Bové J, Prou D, Perier C, Przedborski S. Toxin-induced models of Parkinson's disease. *NeuroRx*. 2005;2:484-494.
62. Burke RE, O'Malley K. Axon degeneration in Parkinson's disease. *Exp Neurol*. 2013;246:72-83.
63. Kearns CM, Cass WA, Smoot K, Kryscio R, Gash DM. GDNF protection against 6-OHDA: time dependence and requirement for protein synthesis. *J Neurosci*. 1997;17:7111-7118.
64. Penney J, Tsurudome K, Liao EH, et al. LRRK2 regulates retrograde synaptic compensation at the Drosophila neuromuscular junction. *Nat Commun*. 2016;7:12188.
65. Mutez E, Nkiliza A, Belarbi K, et al. Involvement of the immune system, endocytosis and EIF2 signaling in both genetically determined and sporadic forms of Parkinson's disease. *Neurobiol Dis*. 2014;63:165-170.
66. Marín I. Ancient origin of the Parkinson disease gene LRRK2. *J Mol Evol*. 2008;67:41-50.
67. Kenmochi N, Kawaguchi T, Rozen S, et al. A map of 75 human ribosomal protein genes. *Genome Res*. 1998;8:509-523.
68. Yoshihama M, Uechi T, Asakawa S, et al. The human ribosomal protein genes: sequencing and comparative analysis of 73 genes. *Genome Res*. 2002;12:379-390.
69. Moriya H. Quantitative nature of overexpression experiments. *Mol Biol Cell*. 2015;26:3932-3939.
70. Manzoni C, Lewis PA. LRRK2 and autophagy. *Adv Neurobiol*. 2017;14:89-105.
71. Wek RC, Jiang HY, Anthony TG. Coping with stress: eIF2 kinases and translational control. *Biochem Soc Trans*. 2006;34:7-11.
72. Woods YL, Cohen P, Becker W, et al. The kinase DYRK phosphorylates protein-synthesis initiation factor eIF2Bepsilon at Ser539 and the microtubule-associated protein tau at Thr212: potential role for DYRK as a glycogen synthase kinase 3-priming kinase. *Biochem J*. 2001;355:609-615.
73. Pavitt GD, Proud CG. Protein synthesis and its control in neuronal cells with a focus on vanishing white matter disease. *Biochem Soc Trans*. 2009;37:1298-1310.
74. Pause A, Belsham GJ, Gingras AC, et al. Insulin-dependent stimulation of protein synthesis by phosphorylation of a regulator of 5'-cap function. *Nature*. 1994;371:762-767.
75. Gingras AC, Raught B, Sonenberg N. eIF4 initiation factors: effectors of mRNA recruitment to ribosomes and regulators of translation. *Annu Rev Biochem*. 1999;68:913-963.
76. Leegwater PA, Yuan BQ, van der Steen J, et al. Mutations of MLC1 (KIAA0027), encoding a putative membrane protein, cause megalencephalic leukoencephalopathy with subcortical cysts. *Am J Hum Genet*. 2001;68:831-838.
77. van der Knaap MS, Leegwater PA, Könst AA, et al. Mutations in each of the five subunits of translation initiation factor eIF2B can cause leukoencephalopathy with vanishing white matter. *Ann Neurol*. 2002;51:264-270.
78. Gully RL, Wood RL. The fine structure of neurons in the rat substantia nigra. *Tissue Cell*. 1971;3:675-690.
79. Domesick VB, Stinus L, Paskevich PA. The cytology of dopaminergic and nondopaminergic neurons in the substantia nigra and ventral tegmental area of the rat: a light- and electron-microscopic study. *Neuroscience*. 1983;8:743-765.
80. Olanow CW, Tatton WG. Etiology and pathogenesis of Parkinson's disease. *Annu Rev Neurosci*. 1999;22:123-144.
81. Gandin V, Topisirovic I. Co-translational mechanisms of quality control of newly synthesized polypeptides. *Translation*. 2014;2:e28109.
82. Jellinger KA. Neuropathobiology of non-motor symptoms in Parkinson disease. *J Neural Transm*. 2015;122:1429-1440.
83. Varidaki A, Mohammad H, Coffey ET. *Molecular Mechanisms of Depression*. London: Elsevier; 2016.
84. Lipton JO, Sahin M. The neurology of mTOR. *Neuron*. 2014;84:275-291.
85. Gerhard DM, Wohleb ES, Duman RS. Emerging treatment mechanisms for depression: focus on glutamate and synaptic plasticity. *Drug Discov Today*. 2016;21:454-464.
86. Collier TJ, Kanaan NM, Kordower JH. Ageing as a primary risk factor for Parkinson's disease: evidence from studies of non-human primates. *Nat Rev Neurosci*. 2011;12:359-366.
87. Poewe W, Seppi K, Tanner CM, et al. Parkinson disease. *Nat Rev Dis Primers*. 2017;3:17013.
88. Postuma RB, Poewe W, Litvan I, et al. Validation of the MDS clinical diagnostic criteria for Parkinson's disease. *Mov Disord*. 2018;33:1601-1608.

SUPPORTING INFORMATION

Additional Supporting Information may be found online in the Supporting Information section.

How to cite this article: Deshpande P, Flinkman D, Hong Y, et al. Protein synthesis is suppressed in sporadic and familial Parkinson's disease by LRRK2. *The FASEB Journal*. 2020;34:14217–14233. https://doi.org/10.1096/fj.202001046R